Electrical Equivalent Circuit Modeling of Various Electrically Small Antennas for Biomedical Applications

Balaka Biswas [iD] [a], Ayan Karmakar [iD] [b]

[a] Indian Institute of Science and Education Research (IISER), Mohall, India.
[b] Semi-Conductor Laboratory (SCL), Deptement of Space, Chandigarh, India.

ABSTRACT

This work outlines various electrically small antennas' design and development activities for biomedical applications. It also covers the electrical modeling aspects of all these miniaturized antennas. Three antennas with different specifications have been discussed with diversified proposed applications. The first example deals with a single frequency (9.45 GHz) on-chip antenna. In contrast, the second one covers an ultra-wideband frequency range (2.5 to 20.6 GHz), and finally, the third antenna targets an application for a 100 GHz band. The size of the first one is 2×2.1 mm2, while the second on-chip antenna occupies an area of about 4.6×11.5 mm2 over the silicon substrate. The third antenna module is developed on LCP substrate, which can be accommodated within a 12.5×27 mm2 area. Though the two on-chip antennas offer the only lower gain of around -29 dBi and -3 dBi, respectively, implementing silicon as a base material paves the way for monolithic integration within a chip. The third candidate exhibits a directive gain of 19-20 dBi with a radiation efficiency of 80% over the 100 GHz band. The highlighted portion of this current research work is to propose empirical modeling of electrically small antennas. The proposed methods claim to be most straightforward in nature. Without applying complicated mathematical jugglery, accessible circuit models are presented for these aforesaid antennas, going to the insight of device physics. A comparative study has been carried out with the proposed model and full-wave simulated results for each antenna to validate the circuit models.

Keywords: ESA, Antenna Modeling, Silicon, OCA, ISM, UWB, THz, Antenna Array, Biomedical.

INTRODUCTION

Electrically small antennas (ESA) are getting paramount importance in recent years. The whole world is running after miniaturization towards compactness, lightweight, and cost-effective circuit realization for handheld devices. Research on this specified field has become attractive in the latest times because of several promising features of ESA keeping synergy with future communication demands, like- fifth-generation mobile communication (5G), millimeter-wave(mmW) communication, IoT (Internet-of-Things), RFID(radio frequency identification system), and above all in numerous biomedical applications for the welfare of mankind, etc. [1-3] Common figure of merits for these small antennas are their radiation efficiency, physical length, electrical size, and radiation quality factor. Though the concept of ESA was proposed in the year 1947-48, however, the practical implementation happened from the mid of the last decade only because of several technological constraints [4-7].

At this moment, while communication engineers have been trying to develop System-On-Chip (SoC) or Antenna-in-Package (AiP) for the last two decades, then ESAs are gaining maximum popularity because of their several salient features, like- lightweight, compact size, low or sufficient gain for short-haul communication, etc. [8-10] Traditionally, all the blocks of RF-SoC can be integrated into a single chip. In contrast, the main radiator is placed outside the chip because of its larger size. This kind of antenna is off-chip in nature and realized by PCB fabrication techniques. Presently, the on-chip versions of the antenna make the system unable to accommodate all the building blocks within a single silicon chip,

including the main radiator. The higher permittivity of silicon ($\epsilon r=11.7$) and lower resistivity make it a lossy medium for EM-waves. Thus, significant attenuation occurs for gain and efficiency factors of the antenna. But, the monolithic integration feature of silicon substrate supersedes all these shortcomings.   On the way to this current development scenario of ESAs, implementing the standard micro-fabrication process electrical modeling prior to the fabrication process will be very much beneficial for any antenna engineers; it will give an overview of the working principle of the radiating element.

Usually, for miniaturization of antenna structures seven basic methods are adopted in designing, such as: meandering [11], looping [12], fractals [13-15], shorting pin [16], loading of reactive elements [17, 18], slot incorporation [19, 20] and stacking (or capacitive loading) [21, 22]. One or more of these techniques can be adopted to realize an efficient small antenna as per the user specifications. But, this complicated design approach can be made very easy enough by implementing the circuit model to understand insight device physics. Several modeling approaches [21-25] of ESAs have already been reported, but complicated mathematics and abstract modeling strategies make them hardly user-friendly. Theoretically, the antenna's gain is directly proportional to its physical dimension or aperture size. The ESA has thus inherently low gain feature. Although, in recent times, researchers have put significant efforts to enhance the gain, bandwidth, and radiation efficiency profiles of the ESA and several other radiation characteristics targeting multifaceted applications, including bio-medical usages [26-31].

In this work, we focus upon two on-chip antennas on silicon substrate targeting 9.45 GHz (X-band) and super wideband, SWB (2.5 to 20.6 GHz) applications along with one miniaturized version of array antenna on a flexible substrate for 100 GHz usages. The on-chip version of the antenna structures is inherent in lower gain profiles. The X-band antenna offers a gain of -29 dBi with 21.07 % radiation efficiency. In contrast, the SWB on-chip antenna exhibits a maximum gain of -3dBi with more than 80 % efficiency except for the notched band. The third item targeting the Terahertz applications for microwave imaging offers a gain of around 19.3 dBi with more than 80% radiation efficiency. The emphasis of the current research work is the electrical modeling of the aforesaid antenna modules in a very easy manner.

1. Antenna design and its electrical equivalent circuit

This section outlines the design and analysis of ESAs along with the electrical modeling aspect as follows:

1.1. ESA-1: On-chip X-band antenna

It is an on-chip antenna using silicon as a base material and targeting bio-telemetry application at 9.45 GHz (ISM band). It can be suitable for inter/intra-chip wireless communication and healthcare applications. Especially in the case of wireless body area network (WBAN), such antenna can be of special attraction. Three salient miniaturization techniques have been adopted here, namely-meandered loop, capacitive loading, and shorting pin concepts. Chip size is about 2.1×2.0 mm2. Standard 0.18 μm technology node has been used as a baseline process. The geometry of the antenna is shown in Fig.1 with detailed dimensions. Here, a partially shielded layer (PSL) is implemented to reduce the size of the antenna as well as enhance its directive gain. This PSL provides a capacitive loading effect and shifts the resonance frequency of the reference antenna from 23 GHz to 11.07 GHz. The size of the antenna is further reduced with a conical-shaped shorting pin connecting the antenna and PSL. This pin shifts the resonance frequency to 9.45 GHz. The gain of the antenna is -29 dBi with 21 % radiation efficiency. The antenna's radiation characteristic (simulated) is shown in Fig.2.

The electrical equivalent model of this miniaturized antenna is proposed in Fig.3. It has basically three distinct segments: feed section (R_f and L_f), resonating/radiator part with TM_{10} mode (L_{10}, C_{10}, and R_{10}), and finally through-silicon oxide via hole (C_{ox}, L_{via} and R_{via}). Finite conductor loss is expressed with the help of R_f and L_f portions. In contrast, the parallel tank circuit is responsible for reserving the EM-energy of the resonator/radiator showing TM_{10} mode. L_{10} and C_{10} together decide the resonance frequency, while R_{10} determines its impedance bandwidth. In this structure, the plated through via-hole configuration is denoted by a parasitic lossy inductor with substrate capacitance (C_{ox}). With the variation of $SiO2$-thickness, this C_{ox} value is changed significantly. It acts as a parallel-plate capacitor between the top metal layer and the bottom ground plane. The via-hole inductance is solely dependent upon the size and shape of the hole and substrate height.
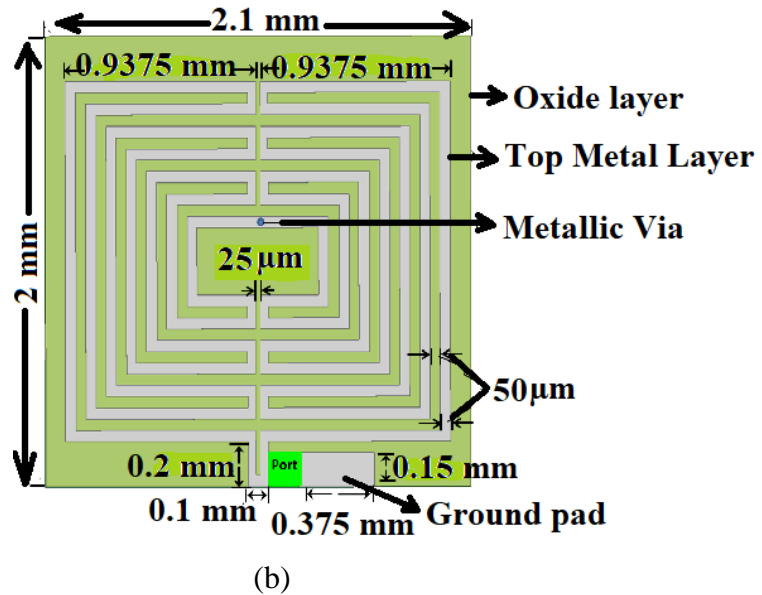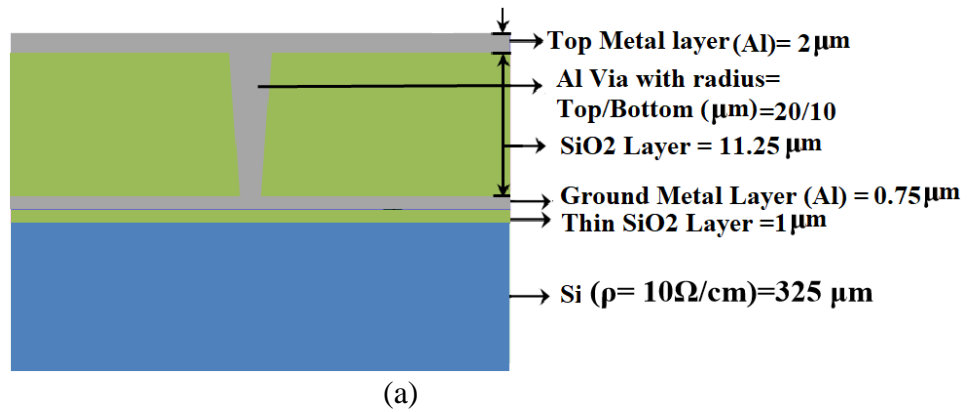
Top Metal layer (Al)= 2 μm

Al Via with radius=
Top/Bottom (μm)=20/10

SiO2 Layer = 11.25 μm

Ground Metal Layer (Al) = 0.75 μm
Thin SiO2 Layer =1 μm

Si (ρ= 10Ω/cm)=325 μm

(a)

2.1 mm

0.9375 mm   0.9375 mm

Oxide layer

Top Metal Layer

Metallic Via

2 mm

25 μm

50 μm

0.2 mm   Port   0.15 mm

0.1 mm   0.375 mm   Ground pad

(b)

Figure 1: (a) Cross-sectional diagram (b) schematic top view diagram and [8].
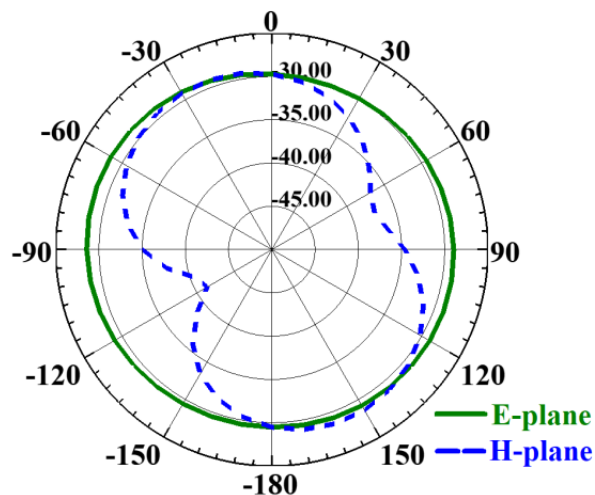
Figure 2: Simulated radiation pattern of the ESA-I in E-plane (φ=0°) H-plane (φ=90°) at 9.45 GHz.

With the parametric extraction techniques, values of all circuit elements have been summarized in Table-I for this model. Fig. 4 shows the close relevance between the circuit modeling and the full-wave simulated result of the antenna. Equation (1) describes mathematically the input impedance of the OCA with all parameters associated with it.

$$Z_{OCA} = Z_f + \frac{1}{Y_{Loop}} + \frac{1}{Y_{Via-hole}} \qquad (1)$$

Where, $Z_f = R_f + j\omega L_f$; $Y_{Loop} = \frac{1}{R_{10}} + \frac{1}{j\omega L_{10}} + j\omega C_{10}$ and $Y_{Via-hole} = j\omega C_{ox} + \frac{1}{R_{Via} + j\omega L_{via}}$.

Freq.(GHz) /Parameter	8	8.57	9	9.45	9.7	10	10.2	10.4	10.5	10.7
Oxide Thickness (µm)	5.25	7.25	9.25	11.25	13.25	15.25	17.25	19.25	21.25	23.25
$R_{10}\,(\Omega)$	250	250	350	275	275	300	300	300	225	225
L_{10} (nH)	0.0687	0.0618	0.0618	0.054	0.0549	0.048	0.048	0.048	0.048	0.041
C_{10} (pF)	0.344	0.229	0.1486	0.344	0.147	0.44	0.39	0.24	0.19	0.73
C_{ox} (pF)	5.58	5.54	5.0678	4.99	4.922	4.97	4.82	4.77	4.7	4.7
L_{via} (pH)	0.565	0.67	0.452	0.678	0.678	0.565	0.565	0.565	0.565	0.565
$R_{via}\,(\Omega)$	31.2	39	76. 5	144	144.3	140	156	159	163	132
$R_f\,(\Omega)$	1	3.8	0.5	0.7	1.1	1.8	1.9	2	1.3	0.5
L_f (nH)	1.085	1.085	1.085	1	1.01	1.117	1.11	1.24	1.24	1.24

Table-I: Optimized parameter for the circuit elements of the ESA-I structure.
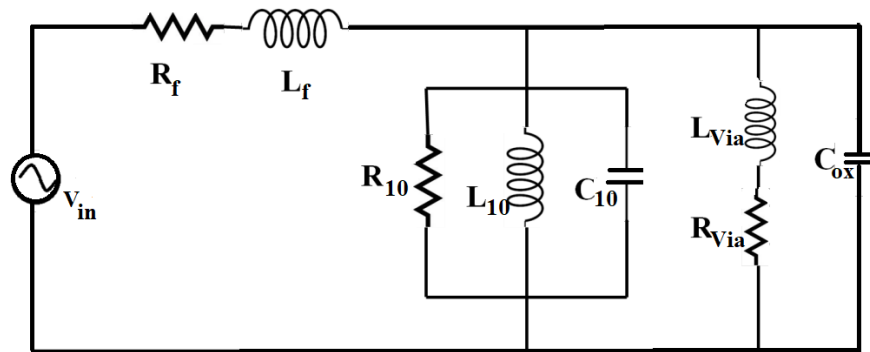

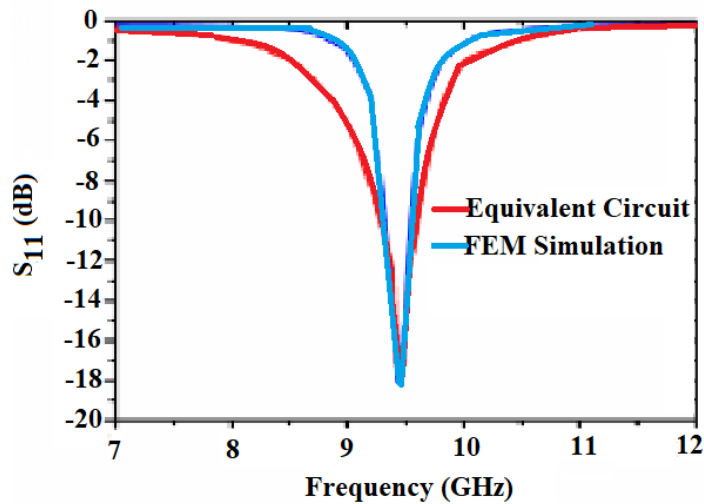
Figure 3: Equivalent circuit model of OCA.

Figure 4: Comparative data analysis of the antenna.

1.2. ESA-II: On-Chip Super Wideband Antenna

This is a miniaturized CPW-fed Ultra-Wide Band (UWB) on-chip monopole antenna with band-notch characteristics. It exhibits a VSWR < 2.0 for the frequency band of 2.5 GHz to 20.6 GHz. It is suitable for the WBAN system and medical imaging application because of its super-wide band feature. This antenna is designed for 675±30 µm thick high resistive silicon (ρ≥8 co-cm, tan=0.01, εr=11.7) substrate. It occupies an area of 8.5×11.5 mm2. Though most of the reported on-chip antennas are for 60 GHz communication [32, 33], the research on UWB antenna using silicon as a substrate is still rudimentary. The specialties of the current work are compact antenna on silicon which covers extended UWB band along

with band-notch capability to mitigate interference issues for X-band uplink satellite communication systems. Here, the main radiating element is an irregular octagonal patch with a rectangular spiral-shaped slot embedded within it. A U-shaped slot is included in the feed-line to achieve the band-notching behavior. Triangular-shaped corners have been etched out from all four corners of the patch to achieve wideband characteristics, and a further rectangular-shaped slot of half-wavelength long is embedded into the main radiating element to attain a super-wideband profile. To get the filtering characteristics a quarter-wavelength ($\lambda g/4$) long U-shaped slot is implemented in the feed-line. The geometry of the whole structure is shown in Fig.5, and all optimized dimensions are listed in Table II. This antenna provides a maximum gain of -3 dBi with more than 80% radiation efficiency except for the notched band. The radiation characteristic of the ESA-II structure is shown in Fig.6.
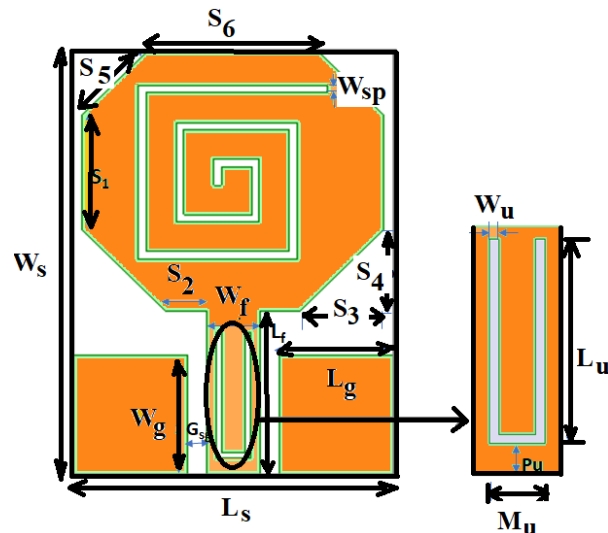

Figure 5: Geometry of ESA-II structure [9].

Mathematically, the input impedance of the on-chip SWB antenna can be describes as follows in terms of Eqn.(2).

$$\mathbf{Z_{Ant}} = \mathbf{Z_f} + \mathbf{Z_{Triangle}} + \mathbf{Z_{slot}} + \frac{\mathbf{1}}{\mathbf{Y_{notch}}} + \mathbf{Z_{UWB}} \qquad (2)$$

Where, $Z_f = R_f + j\omega L_f$; $Z_{slot} = j\omega L_2 + \frac{1}{j\omega C_2}$; $Z_{Triangle} = j\omega L_1 \left\| \frac{1}{j\omega C_1} \right.$; $Z_{UWB} = \sum_{i=4}^{7} \left[R_i \left\| j\omega L_i \left\| \frac{1}{j\omega C_i} \right. \right. \right]$ and $Z_{notch} = R_3 + j(\omega L_3 - \frac{1}{\omega C_3})$.

Circuit modeling of this on-chip antenna is proposed in Fig. 7. It has several segments which explicitly describe the insight device operations. Actual UWB operation can be thought of as a cascaded version of multiple resonant circuits, which are interlinked with each other. Fundamental resonance mode TM_{10} of each resonator corresponds to the values of its constituents, i.e., L_{10}, R_{10}, and C_{10}. These are designated here as (R_4, C_4, L_4); (R_5, C_5, L_5); (R_6, C_6, L_6) and (R_7, C_7, L_7) set. Then four corners of the patch are cut to increase the gain and enhance the impedance bandwidth. These corners are represented by a parallel tank circuit (L1 parallel C_1), and with this, the spiral-shaped half-wavelength long slot is denoted by a series resonant circuit (L_2 & C_2) elements.

For the band notch characteristics, a series RLC resonant circuit (R_3, L_3, and C_3) is connected in parallel with the actual UWB-antenna circuits. The values of L_3 and C_3 are determined by the notch-frequency, whereas R3 dictates its bandwidth. The CPW-feed line is represented here by R_f and L_f, showing the finite conductor loss phenomena for metallization. Table- III summarizes all values of circuit elements for Fig. 7.
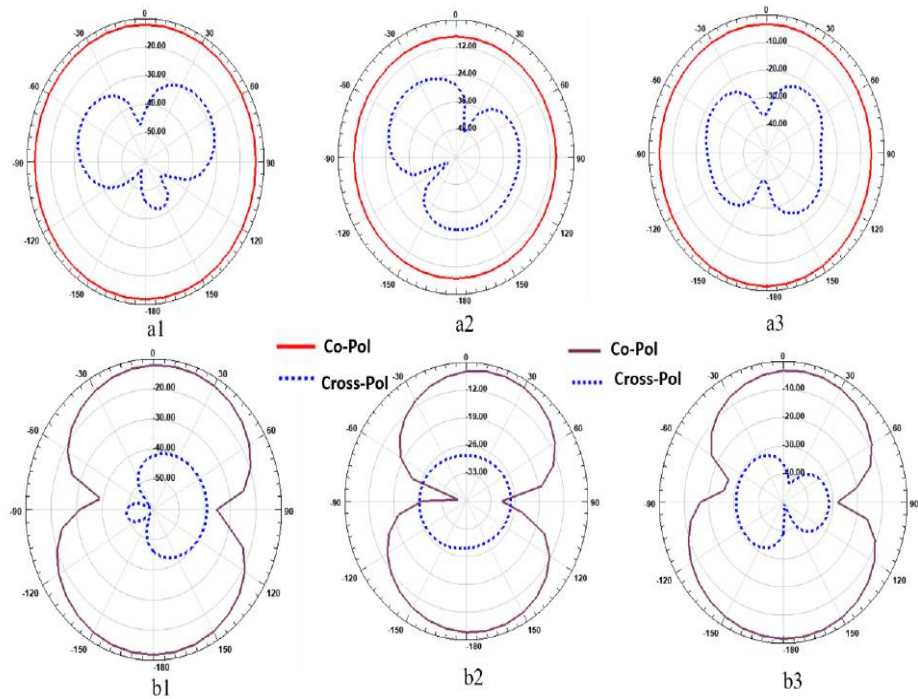
Figure 6: Simulated H-plane radiation pattern at (a1) 8.24 GHz (a2) 10 GHz (a3) 16 GHz and E-plane radiation pattern at (b1) 8.24 GHz (b2) 10 GHz (b3) 16 GHz.
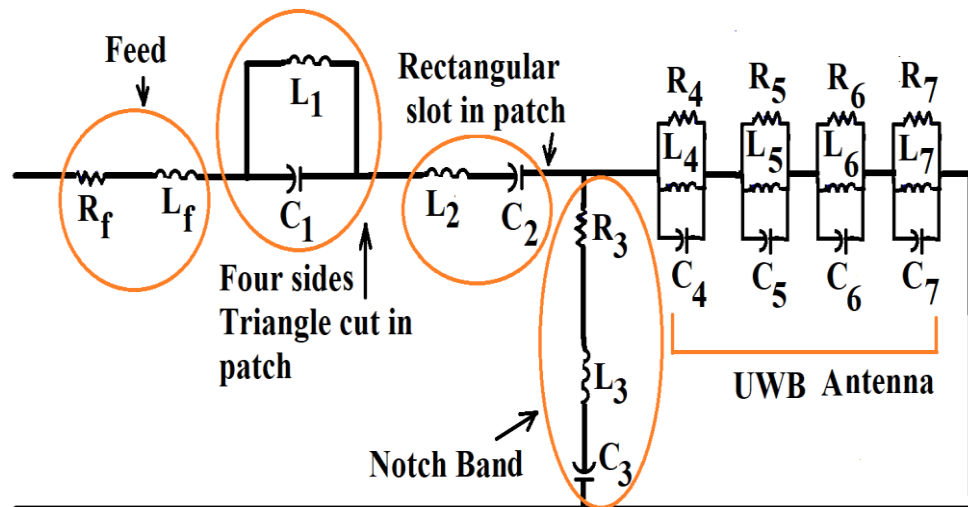

Figure 7: Electrical equivalent circuit of ESA-II.

Table-II: Optimized parameters for the proposed ESA-II.					
Serial No.	Parameters	Values	Serial No.	Parameters	Values
1.	L_s	8.5	10.	P_u	0.5
2.	W_s	11.5	11.	W_{sp}	0.2
3.	L_g	3.04	12.	G_{sg}	0.51
4.	W_g	3.3	13.	S_1	3.1
5.	L_f	4.5	14.	S_2	1.1
6.	W_f	1.4	15.	S_3	2.2
7.	M_u	0.9	16.	S_4	2.2
8.	L_u	3.4	17.	S_5	2.4
9.	W_u	0.15	18.	S_6	4.6

Table-III: Equivalent circuit parameters values of Antenna II.

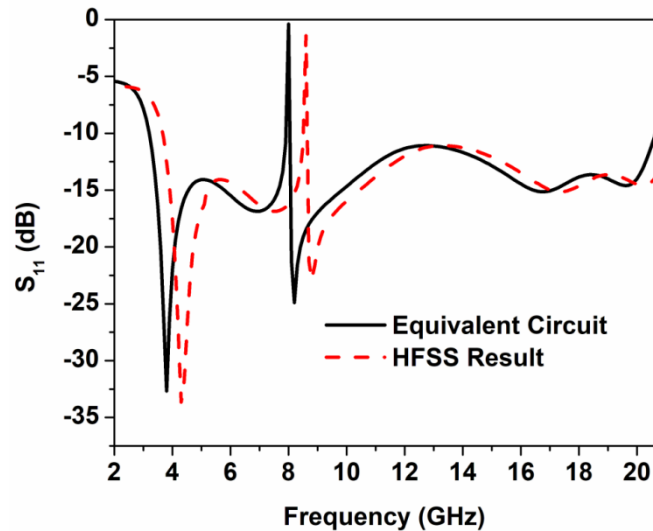| Serial No.	Parameters	Values	Serial No.	Parameters	Values
1.	R_f	15Ω	11.	L_4	0.75nH
2.	L_f	1H	12.	C_4	3.2pF
3.	L_1	75pH	13.	R_5	51Ω
4.	C_1	0.65pF	14.	L_5	0.63nH
5.	L_2	5pH	15.	C_5	1.08pF
6.	C_2	100nF	16.	R_6	63Ω
7.	R_3	0.2Ω	17.	L_6	0.18nH
8.	L_3	45nH	18.	C_6	1.028pF
9.	C_3	8.8fF	19.	R_7	55Ω
10.	R_4	61Ω	20.	L_7	0.6nH
			21.	C_7	1.29pF

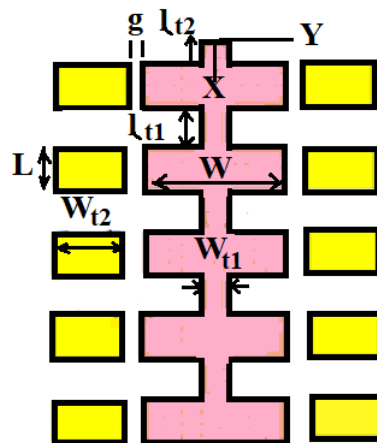Figure 8: Comparison of the circuit modeling and HFSS results.

Figure 9: Geometry of the RMAA [34].

It is a parasitic-element loaded rectangular microstrip antenna array (RMAA) with a very high gain feature on a 4-mil thick LCP (Liquid Crystal Polymer) substrate for 100 GHz application. A high peak gain of around 19.3 dBi has been achieved with the planar configuration having five elements connected in cascade with series feeding. Each of these elements excites two parasitic patches placed on both sides of the non-radiating edges of the primary patches. The structure can be wrapped or conformed over any substrate, and its size is only 12.5×27 mm2. The geometry of the array is shown in Fig.9 with detailed dimensions as specified in Table IV. Implementing parasitic patches at the non-radiating edges of the main patch array effectively enhances the aperture size of the array structure, which in turn increases the gain of the antenna. The radiation pattern of the array structure is shown in Fig.10. The array offers a very high gain with a radiation efficiency of 80 %.

Table IV: Optimized dimension of RMAA		
Variables	Without parasitic elements (µm)	With parasitic elements (µm)
L	2489	2489
W	3078	3078
l_{t1}	1293	1293
l_{t2}	2685	2685
w_{t1}	690	500
w_p	-	1539
g	-	200
h	100	100

This array antenna consists of five main radiating elements, whose resonance frequency is determined by L_{10} and C_{10} of parallel-tank circuits, as shown in Fig. 11. The impedance bandwidth of this resonance for TM_{10} mode is determined by its non-zero value of resistance (R_{10}). Individual radiating elements are connected by a series fed transmission-line segment, which is expressed as a parallel combination of a lossy inductor and a capacitor. The current distribution between radiating elements is expressed as Lij (where, i=1 to 4, and j=2 to 5) with finite conductance (R_{ij}). Parametric capacitances between these elements are expressed by C_{ij}. Parametric elements responsible for enhancing the peak gain of the whole array are expressed by leaky capacitors (C_p and R_p) with an extra parasitic capacitance (C_g). All the optimized circuit parameters have been summarized in Table V. The input impedance, ZRMAA of the array antenna, is given by Eqn. (3). Fig.12 compares the performance of the circuit modeling with FEM simulated results. It shows a close matching.

$$Z_{RMAA} = Z_f + Z_{mainpatch} + Z_{Coupling} + Z_{Parasitic-patch} \tag{3}$$
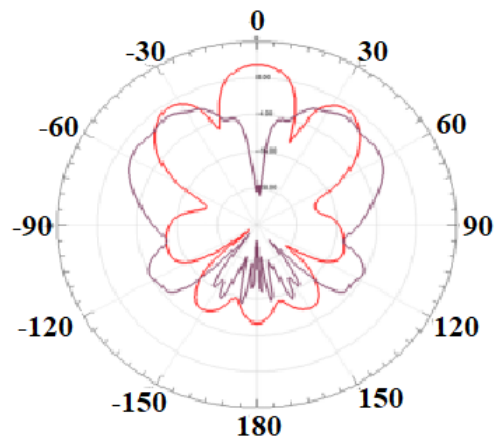
Where, $Z_f = R_f + j\omega L_f$

$$Z_{mainpatch} = \sum_{i=1}^{5}[R_{10}^i \left\| j\omega L_{10}^i \right\| \frac{1}{j\omega C_{10}^i}] \tag{4}$$

$$Z_{Coupling} = \sum_{i=1}^{4}\sum_{j=2}^{5}[\frac{1}{j\omega C_{ij}} \| \{R_{ij} + j\omega L_{ij}\}] \tag{5}$$

$$Z_{Parasitic-patch} = \sum_{i=1}^{5}[[\{R'_{Pi} \left\| \frac{1}{j\omega C'_{Pi}}\} + \frac{1}{j\omega C'_{gi}}] \| [\{R_{Pi} \left\| \frac{1}{j\omega C_{Pi}}\} + \frac{1}{j\omega C_{gi}}]] \tag{6}$$
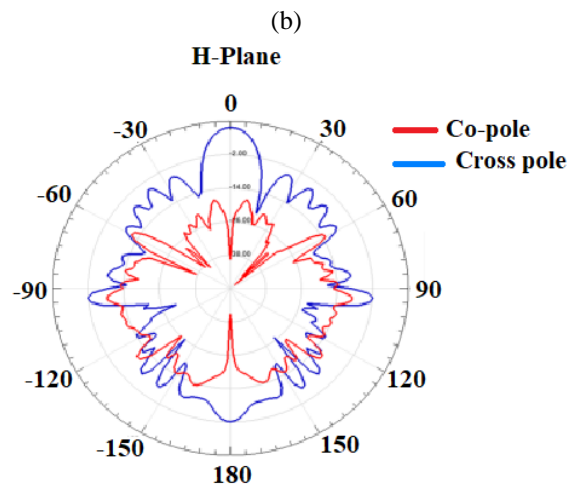
(a)

E-Plane

(b)

H-Plane

Figure 10: Simulated radiation pattern of the RMAA structure in (a) E-plane and (b) H-plane at 100 GHz.
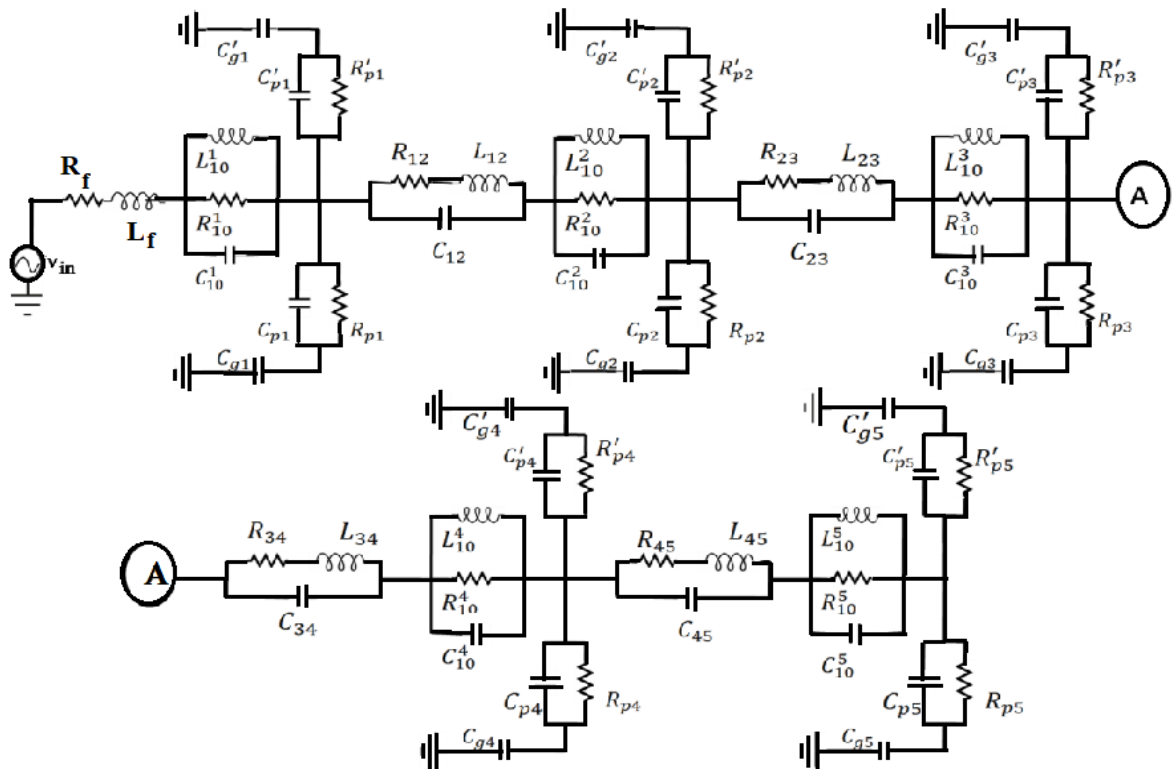

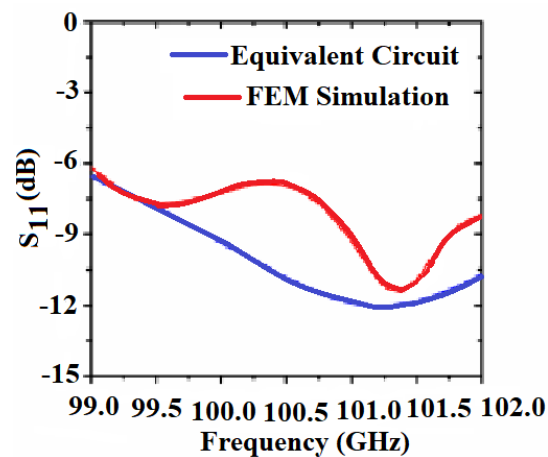Figure 11: Equivalent circuit of the 100 GHz- rectangular Micro strip antenna array.

Figure 12: Comparative data analysis of ESA-III.

Table V: Optimized Electrical parameters of 100 GHz array

Variables	Values	Variables	values
R_f	0.01 Ω	R'_{pi}	161.12 Ω
L_f	54 pH	C_{gi}	16.45 pF
L^i_{10}	4.28 pH	C_{pi}	16.45 pF
C^i_{10}	0.591 pF	R_{pi}	161.12 Ω
R^i_{10}	44 Ω	R_{ij}	55.6 Ω
C'_{gi}	16.45 pF	L_{ij}	100 pH
C'_{pi}	16.45 pF	C_{ij}	7.4 pF

The performance of the proposed electrically small antennas has been compared with other recently reported relevant research works from various renowned groups worldwide, as summarized in Table-VI.

Table-VI: Performance comparison of proposed antennas with other reported works.

References	Antenna substrate	Realization process	Operating frequency(GHz)	Size	Gain(dBi)
[14]	Ultralam3850HT	PCB technique	2.45	0.045λ×0.045λ	-41.8
[15]	Ultralam3850HT	PCB technique	2.45	0.16λ×0.10λ	-30.61
[26]	Felt	Customized technique	0.9/2.45	0.19λ×0.19λ	2.38
[27]	Felt	Customized technique	2/5.8	0.57λ×0.57λ	9.86
[28]	Ultralam-3850	PCB technique	2.45	0.618λ×0.618λ	6.58
[29]	Jeans	Customized technique	0.9 to 6	0.72λ×0.57λ	2.44
[30]	Standard rubber	Customized technique	0.9	0.0007 λ³	8.13
[31]	Flexible substrate	Customized technique	1.4 to 1.6, 1.85 to 2.4, and 3.4 to 11.6	80×70 mm²	2 to 6
[29]	Cotton fabric	Customized technique	1.1 o 8.6	54×36 mm²	8
[35]	Rogers RO3003	PCB technique	2.45	0.16λ×0.125λ	-10
This work: ESA-I	Silicon substrate(ρ=10 Ω-cm)	0.18 μm CMOS process	9.45	0.062λ×0.0651λ	-29
This work: ESA-II	High resistive silicon(ρ=8 kΩ-cm)	Standard micro-fabrication process	2.5 to 20.6	0.138λ×0.345λ	-3
This work: ESA-III	Ultralam3850HT	PCB technique	100	12.6×27 mm²	+19.3

2. Fabrication of Antennas

The first two categories of antennas have been realized on silicon substrate using standard micro-fabrication processes, while the third one is developed on a flexible substrate called LCP, which is biocompatible in nature.Fig.13 depicts the fabricated prototypes.
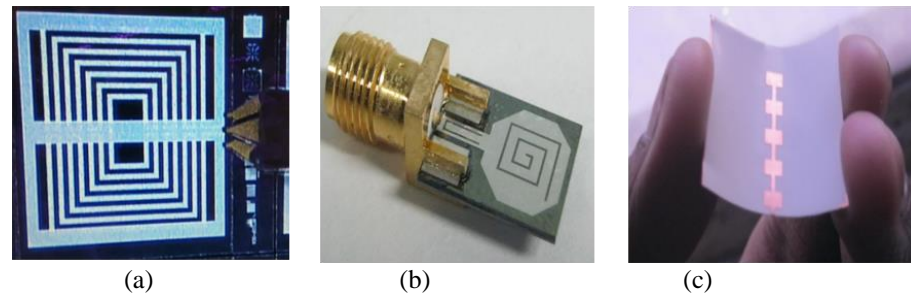
(a)	(b)	(c)

Figure 13: Fabricated prototypes of the (a) ESA-I (b) ESA-II (c) ESA-III.

CONCLUSION

The design of this current research work has summarized the design and development of three types of electrically small antennas. All the miniaturized antennas discussed in this article target various facets of biomedical engineering in demand of the future healthcare system. Especially, wireless body area networks (WBAN) require such ESAs in a large quantity with repeatable promising features. Electrical modeling is proposed in each case to envisage device performance and better understand design parameters. Hence, insight device physics becomes transparent to the designer. Three antennas with different electrical specifications and diversified base substrates (high resistive silicon, low resistive silicon, liquid crystal polymer, etc.) have been considered to validate the proof of concept. Further, the vector-fitting curve method and various network synthesis techniques can be applied to formulate the closed-form equations of circuit elements' values as a function of frequency.

REFERENCES

[1] Best SR, Hanna DL. A performances comparison of fundamental small-antenna design. IEEE Antennas propagation. 2010; 52(1): 47-70. DOI: 10.1109/MAP.2010.5466398

[2] Oleksiy SK, Breinbjerg O, Yaghjian AD. Electrically small magnetic dipole antennas with quality factors approaching the chug lower bound. IEEE Antennas Propagation. 2010; 58(6):1898-1906. DOI: 10.1109/TAP.2010.2046864

[3] Biswas B, Ghatak R, Poddar DR. UWB monopole antenna with multiple fractal slots for band notch characteristic and integrated Bluetooth functionality. J Electr Waves Application. 2015;29(12):1593-1609. DOI:10.1080/09205071.2015.1054521

[4] Wheeler H. Small antennas. IEEE Antennas propagation. 1975; 23(4):462-469. DOI:10.1109/TAP.1975.1141115

[5] Wheeler HA. Fundamental limitations of small antennas. IEEE Antennas Propagation. 1947; 35(12):1479-1484. DOI:10.1109/TAP.1975.1141115

[6] Chu LJ. Physical limitations of Omni-directional antennas. *J Applied Physics*. 1948; 19:1163-1175. DOI:10.1063/1.1715038

[7] Fujimoto K, Morishita H. Modern small antennas. *Cambridge University press.* New York, U K; 2013.

[8] Singh H, Mandal S, Mandal SK, Karmakar A. Design of miniaturized meandered loop on-chip antenna with enhanced gain using shorted partially shield layer for communication at 9.45 GHz. IET Microwaves antennas propagation. 2019; 13(7):1009-1016. [Accessed 2022 Jan 28]. Available from: https://ietresearch.onlinelibrary.wiley.com/doi/pdf/10.1049/iet-map.2018.5974

[9] Mandal S, Karmakar A, Singh H, Mandal SK, Mahapatra R, Mal AK. A miniaturized CPW-fed on-chip UWB monopole antenna with band notch characteristic. Intern J Microwave Wireless technolog. 2020; 12(1):95-102. DOI:10.1017/S1759078719000941

[10] Karmakar A, Singh K. Si-RF Technology. Springer; 2019.

[11] Nassar IT, Weller TM. An electrically small meandered line antenna with truncated ground plane. Radio and wireless symposium (RWS). 2011; 94-97. DOI:10.1109/RWS.2011.5725417

[12] Polívka M, Holub A. Electrically small loop antenna surrounded by a shell of concentric split loops. Proceedings Fourth Europ Conference Antennas Propagation. 2010; 1-3.

[13] Biswas B, Ghatak R, Poddar DR. A Fern fractal leaf inspired wideband antipodal Vivaldi antenna for microwave imaging system. IEEE Transactions Antennas Propagation. 2017;65(11); 6126-6129. DOI:10.1109/TAP.2017.2748361

[14] Biswas B, Karmakar A. Chanda V. Hilbert curve inspired miniaturized MIMO antenna for wireless capsule endoscopy. AEU-International J Electro Communicat. 2021; 137. DOI: 10.1016/j.aeue.2021.153819

[15] Biswas B, Karmakar A, Chandra V. Fractal Inspired Miniaturized Wideband Ingestible Antenna for Wireless Capsule Endoscopy. AEU-International J Electro Communicat. 2020; 120. DOI:10.1016/j.aeue.2020.153192

[16] Chapari A, Nezhad AZ, Firouzeh ZH. Analytical approach for compact shorting pin circular patch antenna. IET Microwaves, antennas and propagation. 2017; 11(11):1603-1608. DOI: 10.1049/iet-map.2017.0248

[17] Booket R, Jafargholi A, Kamyab M, Eskandari H, Veysi M, Mousavi SM. A compact multi-band printed dipole antenna loaded with single-cell MTM. IET Microwaves Antennas Propagation. 2012 ; 6(1) :17-23. DOI:10.1049/iet-map.2010.0545

[18] Wang L, Zhang R, Zhao CL, Chen X, Fu G, Shi XW. A novel wide band miniaturized microstrip patch antenna by reactive loading. Progress electromagnetic Research C. 2018; 85(1):51-62. DOI:10.2528/PIERC18051603

[19] Mitra D, Ghosh B, Sarkhel A, Bhadra Chaudhuri SR. A miniaturized ring slot antenna design with enhanced radiation characteristics. IEEE Transactions Antennas Propagation. 2016; 64(1):300-305. DOI:10.1109/TAP.2015.2496628

[20] Patel RH, Desai A, Upadhyaya TK. An electrically small antenna using defected ground structure for RFID, GPS and IEEE 802.11 a/b /g /S applications. Progress Electromagnetic Research Letters. 2018; 75(1):75-81. DOI:10.2528/PIERL18021901

[21] Scardelletti MC, Ponchak GE, Merritt S, Minor JS, Zorman CA. Electrically small folded slot antenna utilizing capacitive loaded slot lines. *IEEE Radio Wireless Symposium* Orlando. 2008; 731-734. DOI:10.1109/RWS.2008.4463596

[22] Kim JH, Ahn CH. Small dual band slot antenna using capacitor loading. Microwave optical technology letter. 2017; 59(9):2126-2131. DOI:10.1002/mop.30693

[23] Pfeiffer C, Grbic A. A circuit model for electrically small antennas. IEEE Transaction Antennas propagation. 2012; 60(4):1671-1683. DOI:10.1109/TAP.2012.2186232

[24] Biswas B, Karmakar A. Electrical equivalent circuit modeling of various fractal inspired UWB antennas. Frequenz. 2021; 75(3-4): 109–116. DOI: 10.1515/freq-2020-0088

[25] Simpson TL, Logan JC, Roway JW. Equivalent circuits for electrically small antennas using LS-Decomposition with the method of moments. IEEE Transaction Antennas propagation. 1975; 37(4):462-469. DOI:10.1109/8.45109

[26] Khalili FK, Haghshenas F, Shahriari A. Wearable dual-band antenna with harmonic suppression for application in medical communication systems. AEU - International Journal of Electronics and Communications. 2020;126. DOI:10.1016/j.aeue.2020.153396

[27] Khalili FK, Shahriari A, Haghshenas F. A simple method to simultaneously increase the gain and bandwidth of wearable antennas for application in medical/communications systems. Internat J Microwave Wireless Technologies. 2020; 13(4): 374-380. DOI: 10.1017/S1759078720001075

[28] Mohamed EA, Omar FA, Ibrahim SM, Mahmoud AA, Sherif RZ. Wearable high gain low SAR antenna loaded with backed all-textile EBG for WBAN applications. IET Microw. Antennas Propag. 2020; 14(8): 791-799. DOI :10.1049/iet-map.2019.1089

[29] Khalili FK. A broadband all-textile wearable MIMO antenna for wireless telecommunication/medical applications. J Textile Institute. 2021; 112(12):2013-2020. DOI:10.1080/00405000.2020.1862492

[30] Shirvani P, Khalili FK, Mohammad HN. Design investigation of a dual-band wearable antenna for tele-monitoring applications. AEU - International J Electronics Communications. 2021; 138. DOI:10.1016/j.aeue.2021.153840

[31] Karimiyan-Mohammadabadi M, Dorostkar MA, Shokuohi F, Shanbeh M, Torkan A. Ultra-wideband textile antenna with circular polarization for GPS applications and wireless body area networks. J Industrial Textile. 2017; 46(8): 1684-1697. DOI:10.1177%2F1528083716631326

[32] Zhang YP, Sun M, Guo LH. On-Chip Antennas for 60-GHz Radios in Silicon Technology. IEEE Transactions Electron Devices. 2005; 52(7):1664-1668. DOI:10.1109/TED.2005.850628

[33] Yang W, MA K, Yeo KS, Lim WM. A 60GHz on-chip antenna in standard CMOS silicon Technology. IEEE Asia Pacific Conference on Circuits Systems. 2012; 252-255. DOI:10.1109/APCCAS.2012.6419019

[34] Biswas B, Karmakar A, Adhikar V. Liquid Crystal Polymer: Potential Bio-compatible Substrate for Antenna Application. Microwave Review. 2021; 21(1): 17-22. [Accessed

2022 Jan 28]. Available from: http://www.mtt-serbia.org.rs/files/MWR/MWR-Vol27No1/Vol27No1-2170-2-Biswas.pdf

[35] Patel R, Upadhyaya T. An electrically small antenna for nearfield biomedical applications. Microw Opt Technol Lett. 2018; 60: 556– 561. DOI:10.1002/mop.31007